Supplementary Material

Even Marius Nordhagen, Henrik Andersen Sveinsson, Anders Malthe-Sørenssen

June 7, 2023

1 Introduction

The supplementary material contains four sections. In section 2 we describe how the contact area is measured. In section 3, some additional information about the failure mechanism is provided. In section 4, the equilibrium shape of the asperity and substrate under various temperatures is discussed. In section 5, we discuss an alternative model for the contact area.

2 Contact area measurement

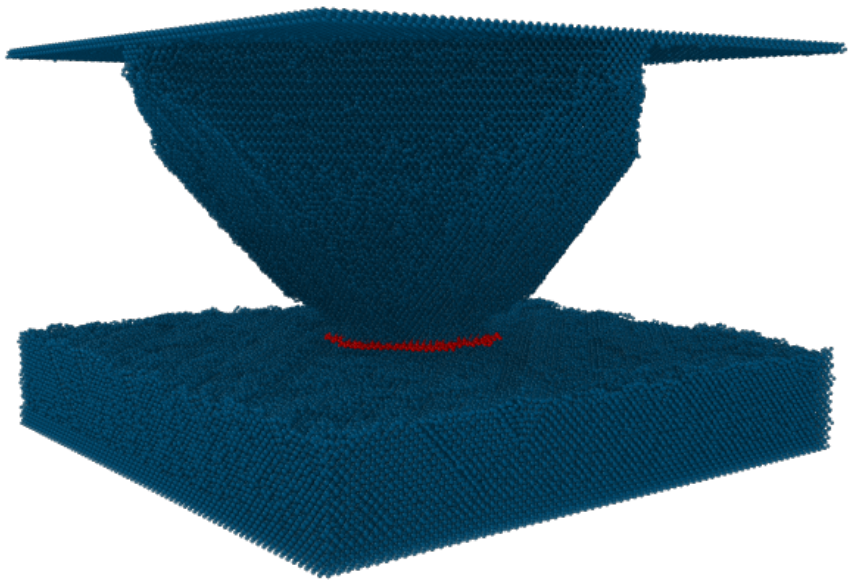

Figure 1: To estimate the contact area between the asperity and the substrate, we analyze a slice close to the substrate. Here we highlight the chosen slice at 55 Å above the lower part of the substrate by red atoms.

The contact area is determined by analyzing the asperity in close proximity to the substrate. A specific slice is carefully selected to ensure that the asperity itself can be distinguished from other structures and peaks on the substrate. For our analysis, we have chosen a slice located at $z = 55$ Å above the lower part of the substrate, with a thickness of 5 Å. This marked slice is depicted in Figure 1.

When slicing the system near the substrate, it is inevitable that surface structure peaks will be included in the slice. To isolate the asperity exclusively, we employ cluster analysis and retain only the largest cluster found within

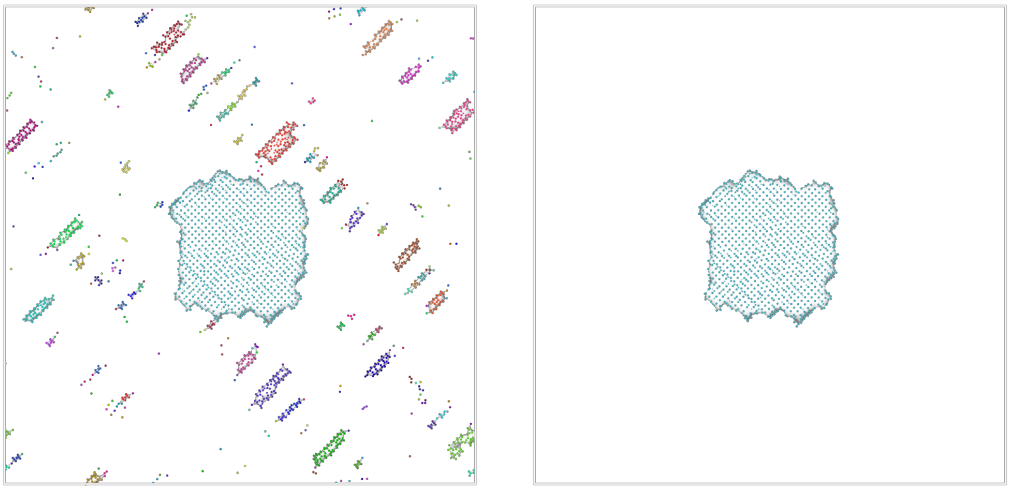

(a) Before removing clusters

(b) After removing clusters

Figure 2: Contact area slice seen from the top before (a) and after (b) small clusters are removed. In (a), atoms are color coded by their cluster-ID.

the slice. The process is illustrated in Figure 2, which displays the slice before and after the removal of smaller clusters through cluster analysis. The cluster radius and surface mesh probe radius are adjusted carefully to ensure accurate identification of the asperity as a single cluster and the surface wrap accurately represents the actual contact area. In this case, the cluster cutoff is set to 2.7 Å, and the probe radius is set to 3.3 Å.

Occasionally, the use of this method may lead to an overestimation of the contact area when peaks on the substrate are connected to the asperity without contributing to the actual contact area. To mitigate this, a coordination analysis is also incorporated. We require all atoms within the asperity to have a coordination number of 4 within a cutoff of 2.5 Å. The estimation of the contact area is performed using Ovito [3].

3 Defects formation under deformation

Figure 3 presents a cross-sectional perspective of the system along the xz direction, offering insights into its pre-deformation state and the deformation process itself. The color-coded visualization distinguishes the atoms based on their specific crystal structures.

Initially, when the lattice grids of the asperity and substrate align perfectly, they amalgamate into a shared crystal structure. However, as the system undergoes deformation, this unified crystal structure undergoes fracturing prior to the ultimate failure of the system. Notably, observations consistently indicate that the onset of cracking predominantly occurs on the left-hand side of the system, as highlighted in the findings of Pham-Ba et al. [1]. Additionally, defects become apparent across the thinnest region of the asperity. Both phenomena are evident in Figure 3b.

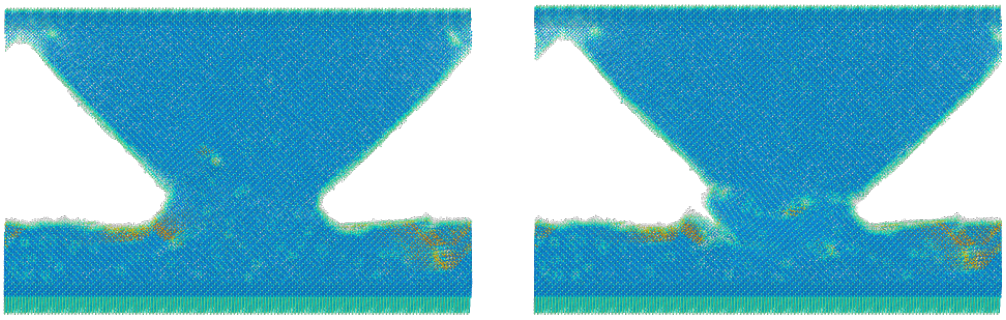

(a) Before deformation (b) During deformation

Figure 3: Cross-section view of the system in xz-direction before (a) and during (b) deformation, with atoms color coded by their crystal structure. Blue color indicates cubic crystal structure, while orange color indicates hexagonal crystal structure.

4 Crystal equilibrium shape

The asperity was carved out to be close to equilibrium, according to Ref. [4]. In figure 4, the shape of the asperity is visualized after 50 ns relaxation at various temperatures. For temperatures 1800, 2000 and 2200 K the asperity keeps its initial shape with minor changes. The changes are more significant for temperature 2300 K, with less distinct facets. When looking at the diamond structure identification for the relaxed asperity, it is apparent that the initial crystal structure (3C-SiC) is still intact for all temperatures.

Figure 3 in the main text showcased the equilibrium shape of the substrate at different temperatures. Notably, it was observed that nano-ribbons emerge at approximately 2000 K. To investigate the formation mechanism behind these nano-ribbons, we have provided a visual representation of the substrate's crystal structure in Figure 5. Upon inspection, we observe that the nano-ribbons arise from a partial transformation of the cubic crystal structure into a hexagonal structure within the substrate. Furthermore, the depth to which the hexagonal structure permeates into the substrate increases as the ribbon size grows larger.

5 Contact area model

In the main text we developed a model for the contact area evolution based on a linear guess for the nucleation energy barrier: $E_b(n) = E_b(0) + an$. We will here consider a more intricate expression for the energy barrier. Rohrer et al. found that the nucleation energy barrier for the formation of a nucleus spanning a facet is proportional to the facet area, $E_b \propto A_F$ [2]. In our system, the area of a facet depends on the number of facets around the asperity and the angle formed between the substrate and the facet. Since the initial contact area is square shaped, we assume that four facets are formed around the asperity. The facets are observed to be normal to the asperity. Using this information, the height and width of a facet can be expressed as $h = nd$ and $w = s + l$, respectively, where d is the thickness of one facet layer, s is the initial contact diameter, and l is the facet length (Figure 6). Therefore, the facet area is given by $A_F(n) = snd + \sqrt{2}(nd)^2$. With a proportionality constant between the facet area and energy barrier, γ, the resulting differential equation is given by

$$\frac{dn}{dt} = f \exp\left(-\gamma \frac{E_b(0) + snd + \sqrt{2}(nd)^2}{k_B T}\right), \tag{1}$$

which can be solved by numerical integration. This model differs from the previous in several ways. While the previous model is a result of approximating the energy barrier with a linear function, this model allows for a second order polynomial fit, but without a constant term. The latter property reflects the fact that there is no initial facet in the notch region, and thus no initial energy barrier. Note that both models reside three fitting parameters (f, $E_b(0)$ and a, and f, $E_b(0)$ and γ). Equation has to be solved numerically, for instance with the Runge-Kutta 4 integration scheme. The model turns out to be unsatisfactory due to the lack of a contact term in the nucleation energy barrier.

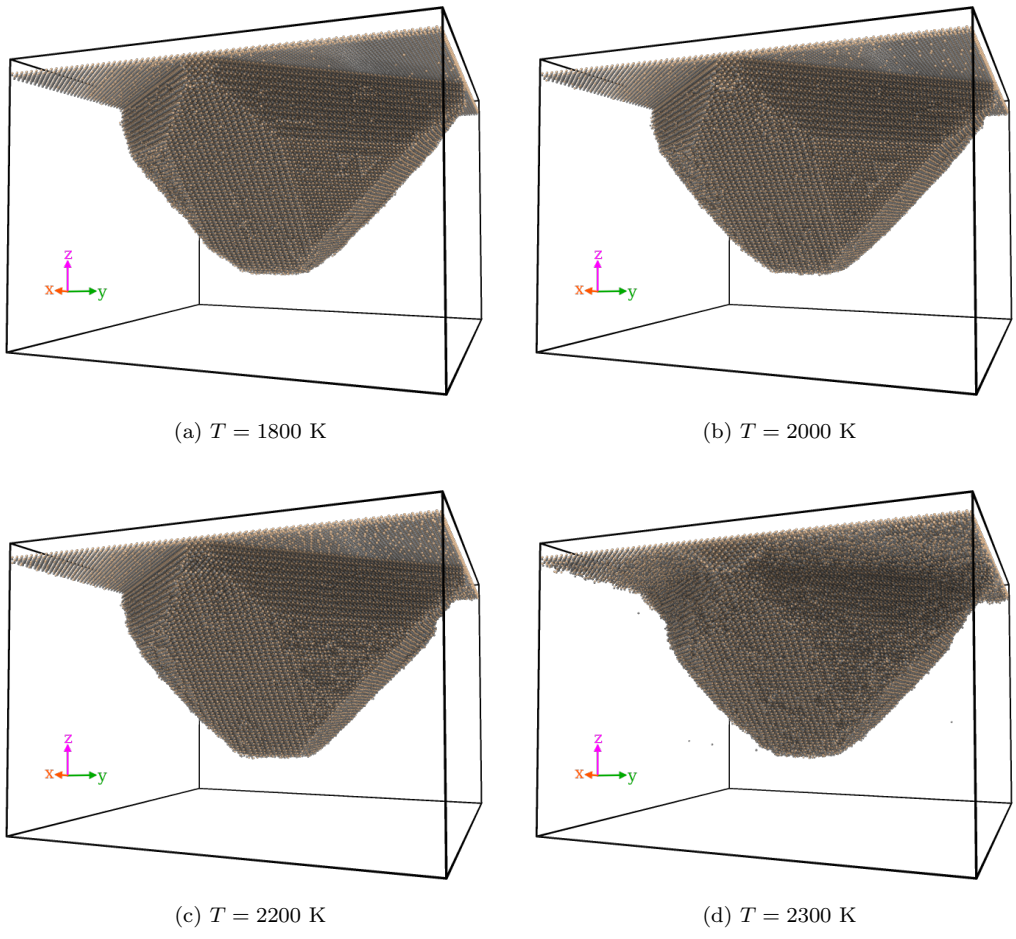

(a) $T = 1800$ K

(b) $T = 2000$ K

(c) $T = 2200$ K

(d) $T = 2300$ K

Figure 4: Asperity shapes after 50 ns of relaxation at various temperatures.

(a) $T = 1800$ K

(b) $T = 2000$ K

(c) $T = 2200$ K

(d) $T = 2300$ K

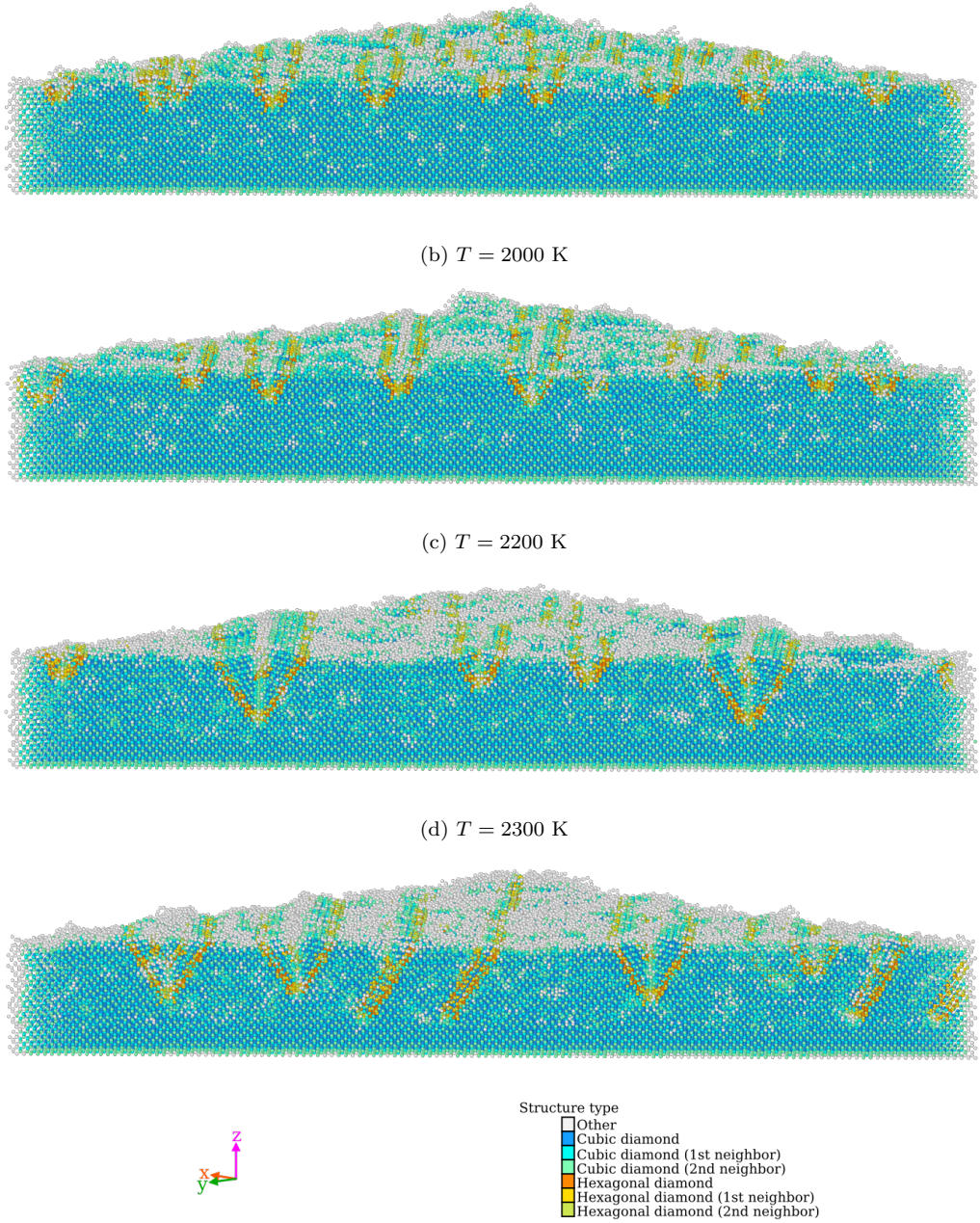

Figure 5: Cross-section view of substrates relaxed for 50 ns at various temperatures. The atoms are color coded based on the crystal structure.

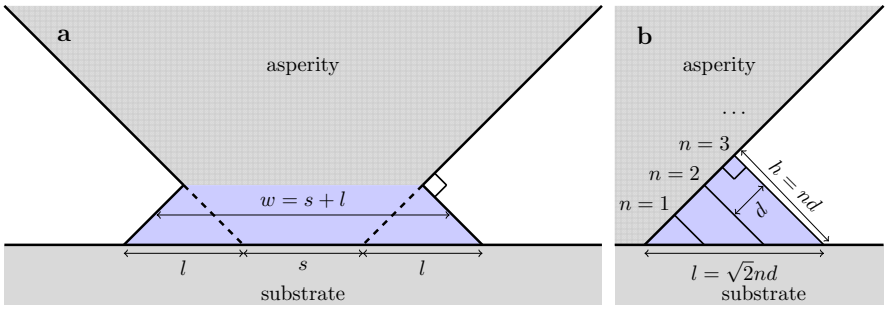

Figure 6: Schematic of facets (blue) in the junction between the asperity and substrate. (a) a facet seen from the front, with middle point width $w = s + l$. (b) a facet seen from the side with height $h = nd$.

References

[1] Son Pham-Ba and Jean-François Molinari. "Creation and evolution of roughness on silica under unlubricated wear". In: *Wear* 472-473 (2021), p. 203648. ISSN: 0043-1648. DOI: 10.1016/j.wear.2021.203648.

[2] Gregory S Rohrer, C Lane Rohrer, and William W Mullins. "Nucleation Energy Barriers for Volume-Conserving Shape Changes of Crystals with Nonequilibrium Morphologies". In: *Journal of the American Ceramic Society* 84.9 (2001), p. 6. DOI: 10.1111/j.1151-2916.2001.tb00965.x.

[3] Alexander Stukowski. "Visualization and analysis of atomistic simulation data with OVITO-the Open Visualization Tool". In: *Modelling and Simulation in Materials Science and Engineering* 18.1 (2010), pp. 015012–015012. DOI: 10.1088/0965-0393/18/1/015012.

[4] Henrik Andersen Sveinsson et al. "Direct Atomic Simulations of Facet Formation and Equilibrium Shapes of SiC Nanoparticles". In: *Crystal Growth & Design* 20.4 (2020), pp. 2147–2152. DOI: 10.1021/ACS.CGD.9B00612.